Wall Shear Stress and Low Density Lipoprotein concentration in stented arteries

Johannes V. SOULIS [1,*], Dimitrios K. FYTANIDIS[1],
Kypriani V. SERALIDOU[1], Varvara C. KARAGKIOZAKI[1], George D. GIANNOGLOU [2]

* Corresponding author: Tel: ++302310994837; Fax: ++302310994837; Email: jvsoulis@med.auth.gr
1: Fluid Mechanics, Demokrition University of Thrace, Greece
2: Cardiovascular Engineering and Atherosclerosis Laboratory,
1st Cardiology Department, Aristotle University of Thessaloniki, Greece

Abstract Current computational analysis results quantify Wall Shear Stress (*WSS*) and its impact on Low Density Lipoprotein (*LDL*) concentration of a fully deployed straight artery stent. Atherosclerosis shows predilection in arterial regions with hemodynamic particularities, as local disturbances of *WSS* in space**,** and locally high concentrations of lipoprotein. The *WSS* and subsequently the *LDL* distribution are important indicators of stent performance. A typical 6.0 mm diameter straight stented artery is used to elucidate the *WSS* and the *LDL* transport under steady flow conditions treating the blood as a non-Newtonian fluid. Struts are 50.0 % embedded into the arterial wall. Emphasis is placed in the *LDL* distribution at the upstream and downstream flow regions of each strut intersection. Reduced *WSS* values are observed towards outlet. At the strut intersections, high *WSS* values are observed possibly causing platelet activation. Prone to plaque development are flow regions located at specific strut intersections (mostly at the vicinity of the curved struts) where increased *LDL* concentration is observed. The maximum *LDL* concentration over the stented artery reaches a value of 3.8 % higher than that at the entrance. The concentration at distal to any strut region was higher than proximal to the strut.

Keywords: Wall Shear Stress, *LDL* Transport, Stented Artery

1. Introduction

In clinical practice stent implantations are widely used to open diseased arteries. Elucidating blood flow and transport of macromolecules in the human cardio-vascular system is essential in understanding the genesis and progression of atherosclerosis (Fatouraee, et al., 1998). Things become even more complicated wherever stented arteries are incorporated. To evaluate the stent performance, researchers have studied various straight artery vessel parameters. These include, amongst others, the thickness of the strut (Dehlaghi, et al., 2008), the shape of the strut connectors (He, et al., 2005) and the deployment ratio (LaDisa, et al., 2003). Furthermore, the arterial curvature influence on Wall Shear Stress (*WSS*) in a stented artery was studied (Zhao, et al., 2010).

The association between low *WSS* and accumulation of macromolecules, leading to atherosclerosis, may be mediated through the effects on mass transport (Soulis, et al., 2008). On the other hand increased *WSS* is related to the reduction of neointimal hyperplasia via inhibition of inflammation (Carlier, et al., 2003). Endothelial cells sense and respond to cyclic mechanical stretching imposed to them through various bio-mechanical factors such as blood static pressure and *WSS*. Regional variation in the permeability of arterial endothelium may contribute to the localization of atherosclerosis (Ogunrinade, et al., 2002). The luminal surface *LDL* concentration is affected by the flow infiltration, which in turn is affected by the deformation of the arterial

wall. An increased permeability to *LDL*, as it is the case of increased plasma *LDL* concentration, increases atherosclerosis (Nielsen, et al., 1996). Higher permeability of the endothelium caused excessive influx of *LDL* to the subendothelial layer. A shear stress-dependent three-pore model applied (Olgac, et al., 2009) for the left coronary artery in its healthy and atherosclerotic state showing that the location of the plaque in the diseased state corresponds to one of the sites with predicted elevated *LDL* concentration in the healthy state.

Nearly all previous research work was concentrated in *WSS* effects upon the accumulation of macromolecules and not in the concentration itself. Henceforth, the *LDL* concentration distribution in stented arteries is not well known. In the current numerical study a typical 6.0 mm diameter straight stented artery, where the struts are 50.0 % embedded into endothelium, is used to elucidate the *WSS* distribution and the *LDL* transport under steady flow conditions. Towards this end, semi-permeable arterial wall (no transmural flow or mass transfer) was used to study the flow and mass transport patterns in stented arteries.

2. Methods

2.1. Geometry and computational grid

The geometry of the employed stented artery computational model has a 3D configuration with 6.0 mm diameter. The strut diameter is 0.1 mm. Figure 1 shows the fully deployed stent geometry. The struts are 50.0 % embedded into the arterial wall, Fig.2. The stented artery computational grid, Fig. 3, is comprised from four quadrants. The Computational Fluid Dynamics (CFD) analysis is performed on one quadrant. Each quadrant contains 1571320 cells or 431470 grid nodes densely located near to endothelium regions. This area is of particular interest. The geometric configuration of the stent has profound effects upon the hemodynamics and subsequently on the *LDL* concentration distribution in the nearby areas.

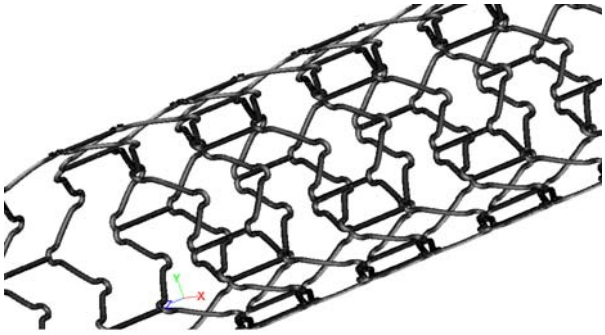

Fig. 1. Stent geometry of the fully deployed artery. Front and rear view projected into a single plane

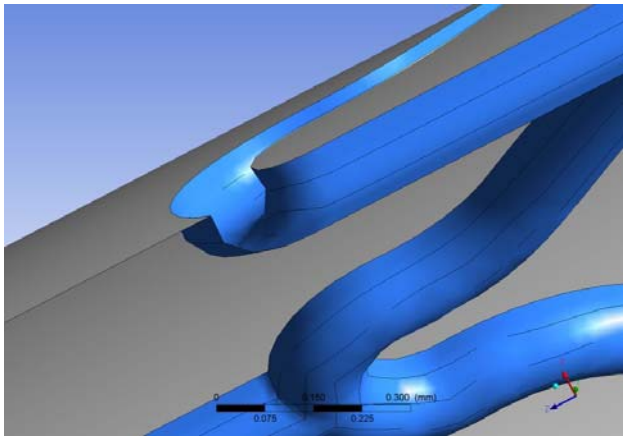

Fig. 2. Stent struts are 50.0 % embedded into the arterial wall

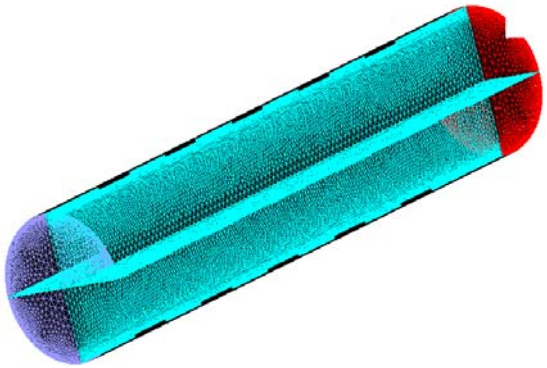

Fig. 3. The computational grid is comprised from four quadrants (CPU time economy)

Furthermore, to efficiently capture the flow and mass pattern distribution at near to endothelium regions, the grid nodes located on the struts are densely located at highly curved areas, Fig. 4.

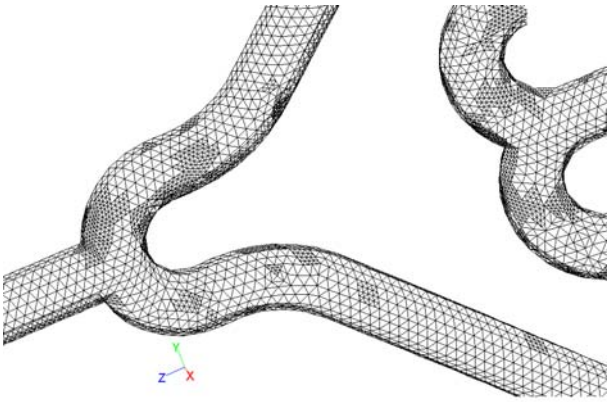

Fig. 4. Computational grid details

2.2. Flow, mass equations and assumptions

All computational grid data as well as all physical flow data determined from the boundary conditions were imported into the main CFD solver (Kelkar, 1989). The numerical code solves the governing Navier-Stokes flow equations and the mass transport equation for the *LDL* in a coupled way. The assumptions made about the nature of the flow are that it is: 3D, steady, laminar, isothermal, with no external forces applied on it. The arterial wall is comprised from non-elastic and permeable material. In their generality the flow governing equations are,

$$\frac{\partial \rho}{\partial t} + \nabla \bullet (\rho \vec{u}) = 0 \qquad (1)$$

ρ (kg/m^3) is the density, t (sec) is the time, $\vec{u}$ (m/s) is the velocity vector. The conservation of momentum (in the general form) is,

$$\frac{\partial}{\partial t}(\rho \vec{u}) + \nabla \bullet (\rho \vec{u}\vec{u}) + \nabla p = \nabla \bullet (\bar{\tau}) + \rho \vec{g} \qquad (2)$$

Here, p (N/m^2) is the static pressure; $\bar{\tau}$ (N/m^2) is the shear stress tensor and $\rho\,\vec{g}$ (N/m^3) the gravitational body force. The shear stress tensor $\bar{\tau}$ is,

$$\vec{\tau} = \mu\left[\left(\nabla \vec{u} + \nabla \vec{u}^T\right)\right] - \frac{2}{3} \nabla \bullet \vec{u} I \qquad (3)$$

μ is the molecular viscosity, I is the unit tensor, and the second term in the right hand side is the effect of the volume dilation. The blood was considered to be non-Newtonian fluid obeying to the power law (Sharma et al., 1992). According to this law the molecular viscosity, now denoted as $\eta(\dot{S})$, is,

$$\eta(\dot{S}) = k e^{\frac{T_o}{T}} \dot{S}^{n-1} \qquad (4)$$

$\dot{S}$ is the shear rate,

$$\dot{S} = \frac{\partial u_i}{\partial x_j} + \frac{\partial u_j}{\partial x_i} \qquad (5)$$

The consistency index k is set 0.00622 (kg-s^n-2/m), the power-law index n is 0.7; T (K) and T_o (K) are local and reference temperatures, respectively. The actual shear stress is,

$$\tau = [\eta(\dot{S})]\,\dot{S} \qquad (6)$$

The solution of the convection-diffusion equation is achieved by,

$$\frac{\partial(\rho C)}{\partial t} + \nabla \bullet (\rho \vec{u} C) + \nabla \bullet \vec{J} = 0 \qquad (7)$$

C (mg/ml) is the *LDL* concentration, $\vec{J}$ is the diffusion flux of *LDL*, which arises due to concentration gradients. The diffusion flux is,

$$\vec{J} = -\rho\, D\, \nabla C \qquad (8)$$

D (m^2/s) is the diffusion coefficient of *LDL* in the mixture.

The blood velocity is assumed to be uniform at the artery inlet. The applied inflow conditions mimic typical blood averaged flow velocity of 0.17 m/s under resting conditions. The blood density is set equal to 1058.0 kg/m^3. For the mass transport solution Eq. (7), a

uniform constant concentration C_o of *LDL* (=1.3 mg/ml) is applied at the artery inlet. At the artery vessel outlet, the gradient of *LDL* concentration along the vessel is set equal to zero (zero flux, Newmann condition) $\frac{\partial C}{\partial s} = 0$, s is the unit vector normal to the outlet surfaces of the artery. The applied endothelium boundary condition at the semi-permeable artery walls is, (Soulis et al., 2008),

$$C_w V_w - D \frac{\partial C}{\partial n} = K C_w \qquad (9)$$

C_w (mg/ml) denotes *LDL* wall concentration, V_w (m/s) the blood infiltration velocity, n the direction normal to the wall. The *LDL* diffusivity D is considered as isotropic and equal to 15.0×10^{-12} m/s^2 and K (m/s) is the permeability coefficient (overall mass transfer coefficient) of *LDL* at the arterial wall. There is a limited amount of experimental data about the actual endothelial permeability K. Thus, specifications of K values are sometimes unreliable. In the current analysis its value is set equal to $2.0\text{x}10^{-10}$ m/s (Wada et al., 2002). Equation (9) states that the net amount of *LDL* per unit area passing from it to the vessel wall is determined by the difference of the mass flow carried to the vessel wall by infiltration flow and the amount of flow which diffuses back to the main vessel flow.

The user defined function capabilities of the numerical code are also incorporated to simulate the mass transport boundary condition across the endothelium, Eq. (9). For a typical satisfactory convergence solution, a total of 400 pseudo-time steps are required. Convergence is achieved when all velocity components, fluid flow, and mass flow changes dropped below 10^{-6}.

3. Results and discussion

3.1. Velocity near endothelium

The near to endothelium flow patterns exhibit complex 3D configuration phenomena. Figure 5 shows the velocity (m/s) streamlines near endothelium for the stented artery. Figures 6 and 7 show the velocity streamlines at very end and at mid-portion region of the stented artery, respectively. Low velocities (less than 0.05 m/s) appear. Streamlines located very close to the struts are highly wavy exhibiting helical flow. However, near to endothelium region the streamlines found at the very end of the straight artery, Fig. 6, are less wavy to those of mid-portion region, Fig.7, which in turn are less wavy to the ones found at the very beginning of the artery (not shown). This is an indication that the blood momentum, within the boundary layer or outside of it, loses its strength from inlet to outlet.

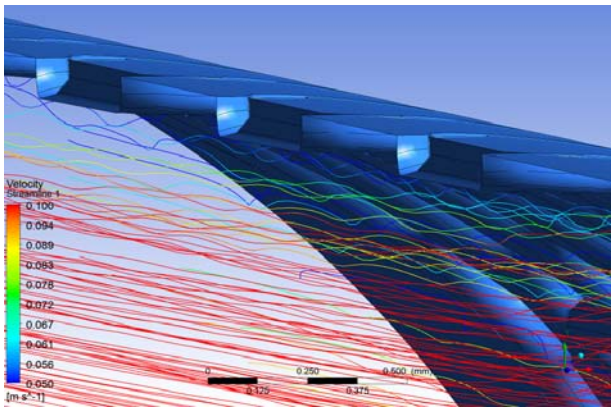

Fig. 5. Velocity (m/s) streamlines near to endothelium of the stented artery. Flow from right to left

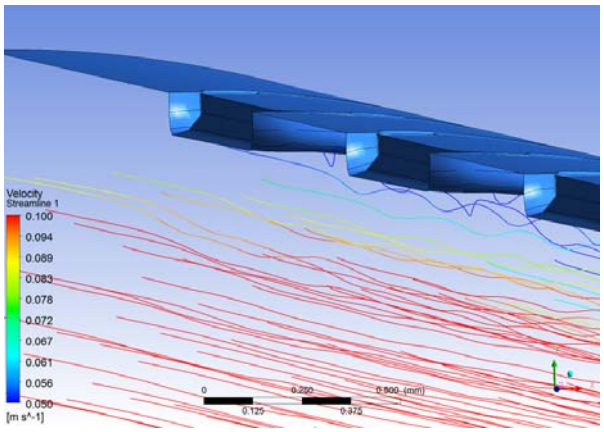

Fig. 6. Velocity (m/s) streamlines near to endothelium at the very end region of the stented artery. Flow from right to left

3.2. Wall Shear Stress

The *WSS* values exhibit low values immediately around the struts, Figs. 8, and 9. However, the endothelium areas covered by low *WSS* values at downstream to struts regions are larger to those found at upstream. Far away from the struts the *WSS* distribution is homogeneous.

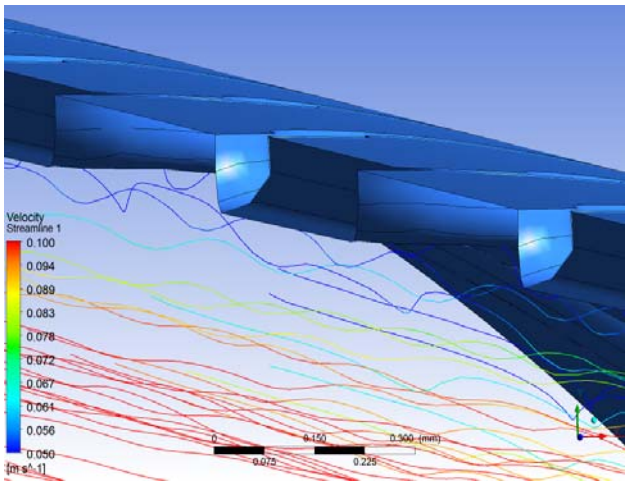

Fig. 7. Velocity (m/s) streamlines near to endothelium at the mid portion region of the stented artery. Flow from right to left

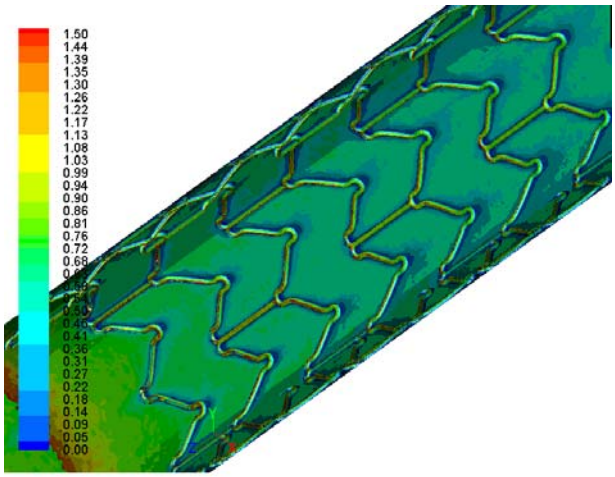

Fig. 8. WSS (N/m^2) contours of the artery (stent and endothelium). Flow from left to right

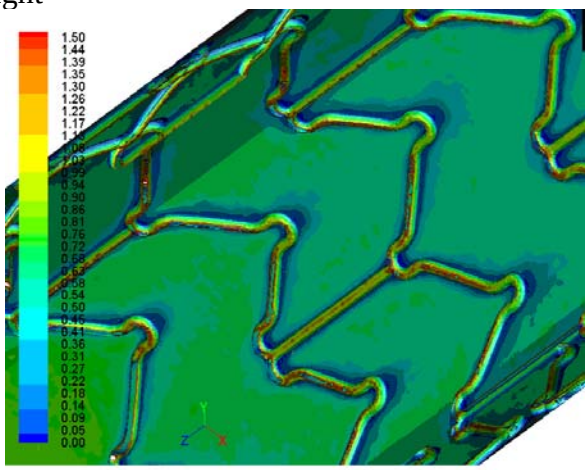

Fig. 9. WSS (N/m^2) contours of the artery (stent and endothelium). Enlarged view. Flow from left to right

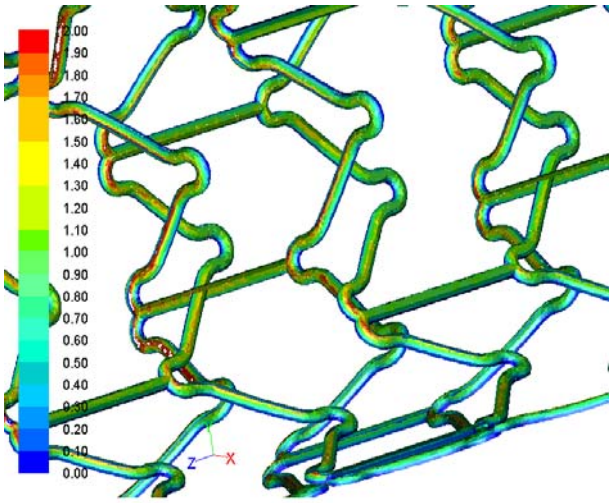

Fig. 10. WSS (N/m^2) contours on struts of the artery. Front and rear view projected in a single plane. Flow from left to right

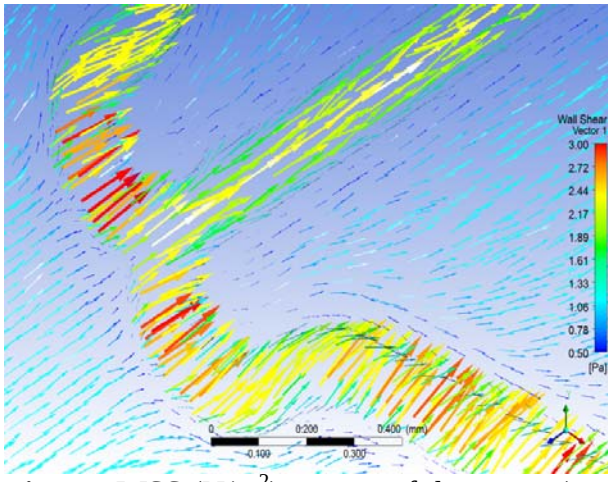

Fig. 11. WSS (N/m^2) vectors of the artery (stent and endothelium)

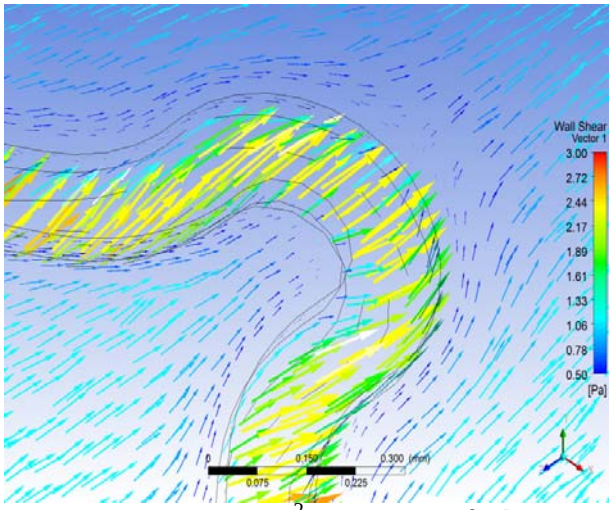

Fig. 12. WSS (N/m^2) vectors of the artery (stent)

The flow exhibits high *WSS* at proximal parts of the stent. Further downstream, the *WSS* is gradually decreased due to momentum reduction. At distal stent parts, low *WSS* patches located immediately downstream to struts, cover larger areas. High *WSS* values (max. 3.0 N/m^2) appear on the struts, Figs. 10, 11 and 12. The *WSS* vector alters its orientation at regions located immediately up and downstream to the struts. This phenomenon increases the 3D complexity of the flow at nearby areas.

3.3. Low Density Lipoprotein transport

The *WSS* magnitude as well as its orientation affects the *LDL* distribution. Typical luminal surface *LDL* concentration C_w contours of the stented artery are shown on Fig. 13. Enlarged views at two distinct strut configurations are shown in Figs. 14 and 15. *LDL* concentration distribution is non-uniform due to stent design. The maximum calculated *LDL* C_w value is 1.35. This value is 3.8 % higher than that at the entrance. Platelet deposition is reported (Duraiswamy, et al., 2008) to be significantly higher at distal to struts regions compared to proximal ones. Furthermore, higher concentration of platelets is reported at the outlet flow region compared to the inlet one, (Duraiswamy, et al., 2008). It must be noted that for the current method analysis the arterial wall was considered to be a healthy tissue. This implies that the physical properties of the endothelium i.e. water infiltration and permeability coefficient is the one of a healthy tissue. Areas with increased *LDL* values are found at the strut proximity regions. However, the concentration at distal to any strut region was higher than proximal to the strut, Figs. 14, 15. In general low *WSS* are regions are to be found at places where high *LDL* appears. However, the high *LDL* regions do not collocate with low *WSS*. In contrary to the *WSS,* the *LDL* concentration pattern is not seriously differentiated from proximal to distal stent parts.

4. Finer scale studies

The length scales addressed in the present study range from the 6.0mm of the arterial diameter, down to the 0.05mm of the 50.0% embedded stent wires. The latter act in a manner similar to eg. roughness elements in heat exchangers (serving to enhance heat transfer) which generate downstream and, possibly, upstream recirculation regions with highly-localized WSS variations. On noting that the erythrocyte diameter is approximately 8.0 microns, our shortest length scale, of 0.05 mm, is seen to be only ~ 6 times this value. Hence, the influence of particulates upon eg. WSS fluctuations associated with their transit, and upon species mixing (both effects not captured in continuum hemodynamics, note) may introduce new modalities into the distributions studied here, in critical regions of the stent already identified as important. Since the current study represents a sensible resolution for a continuum model, there is thus a motive for addressing individual erythrocyte behavior, in a finer-scale model using, a class of solver better adapted to large numbers of Lagrangian particles (erythrocytes). For such studies, perhaps, a Lattice Boltzmann solver would be appropriate. Indeed, experience with these is that eg. predicted residence times are less than with continuum models.

5. Conclusions

The current computational analysis results quantify the *WSS* and its impact on *LDL* concentration of a fully deployed straight artery stent with struts embedded 50.0 % into the arterial wall. *WSS* plays an important role in the wall concentration of the *LDL*. Reduced *WSS* values are observed towards outlet. Increased permeation of *LDL* concentration at specific regions is observed. Prone to plaque development are flow regions located at specific strut intersections (mostly at the proximity of the struts) where increased *LDL* concentration is observed. The maximum *LDL* concentration over the stented artery reaches a value of 3.8 % higher than that at the entrance. The concentration at distal to any strut region was higher than proximal to the strut. In contrary to *WSS,* the *LDL* concentration pattern is not seriously differentiated from proximal to distal stent parts. The paths of the velocity in the proximity to the endothelium region might be the most important factor for elevated *LDL* concentration.

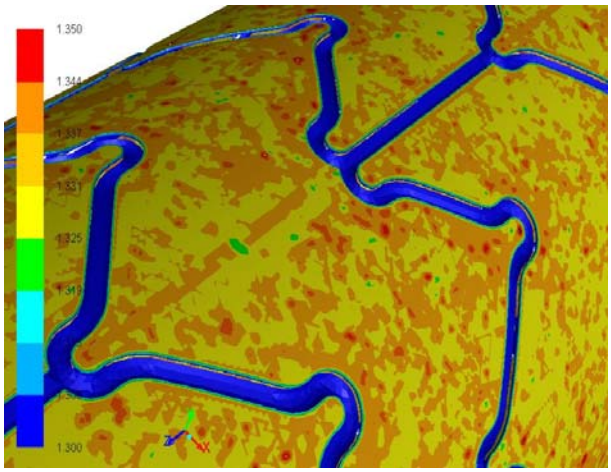

Fig. 13. Luminal surface *LDL* concentration C_w contours of the stented artery. Flow from left to right

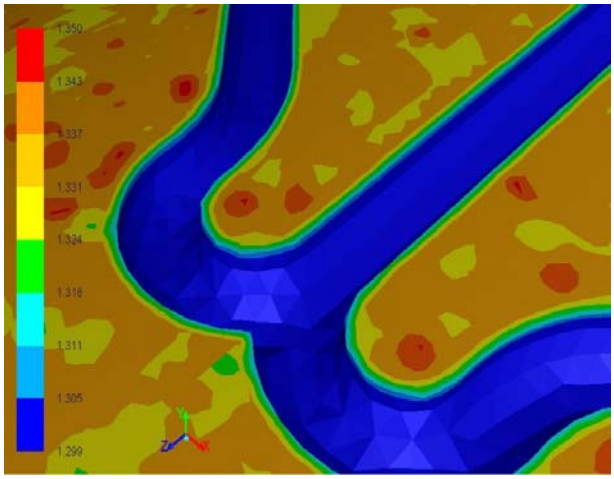

Fig. 14. Luminal surface *LDL* concentration C_w contours of the stented artery. Enlarged view. Flow from left to right

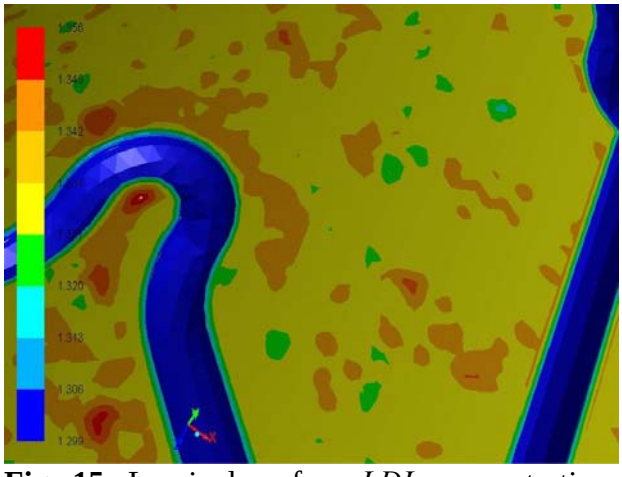

Fig. 15. Luminal surface *LDL* concentration C_w contours of the stented artery. Enlarged view. Flow from left to right

References

Carlier, S.G., van Damme, L.C.A., Blommerde, C.P., Wentzel, J.J., Langehove, G., Verheye, S., Kockx, M.M., Knaapen, M.W.M., Cheng, C., Gijsen, F., Duncker, D.J., Stergiopulos, N., Slager, C.J., Serruys, P.W., Krams, R., 2003. Augmentation of wall shear stress inhibits neointimal hyperplasia after stent implantation-Inhibition through reduction of inflammation? Circulation, 107(21), 2741-2746.

Dehlaghi, V., Shadpoor, M.T., Najarian, S., 2008. Analysis of wall shear stress in stented coronary artery using 3D computational fluid dynamics modeling. Journal of Materials Processing Technology, 197(1-3), 174-181.

Duraiswamy, N., Cesar, J.M., Schoephoerster R.T., Moore, J.E. Jr., 2008. Effects of stent geometry on local flow dynamics and resulting platelet deposition in an in vitro model. Biorheology., 45(5):547-61.

Fatouraee, N., Deng, X., De Champlain, A., Guidoin, R., 1998. Concentration polarization of low density lipoproteins (LDL) in the arterial system, Ann. NY Acad. Sci., 11(5), 137-146.

He, Y., Duraiswamy, N., Frank, A.O., 2005. Blood flow in stented arteries: A parametric comparison of strut design patterns in three dimensions. Journal of Biomechanical Engineering-Transactions of the ASME, 127(4), 637-647.

Kelkar, K.M., 1989. Derivation of pressure and continuity equations for Fluent/bfc. Lebanon NH: Creare Inc.

LaDisa, J.F., 2003. Stent design properties and deployment ratio influence indexes of wall shear stress: a three dimensional computational fluid dynamics investigation within a normal artery. Journal of Applied Physiology, 97(1), 424-430.

Nielsen, L.B., 1996. Transfer of low density lipoprotein into the arterial wall and risk of atherosclerosis. Atherosclerosis, 123(1-2), 1-5.

Ogunrinade, O., Kameya, G.T., Trusky, G.A., 2002. Effect of fluid shear stress on the

permeability of the arterial endothelium. Ann. Biomed. Eng. 30(4), 430-460. Review.

Olgac, U., Poulikakos, D., Saur, S.C., Alkadhi, H., Kurtcuoglu, V., 2009. Patient-specific three-dimensional simulation of LDL accumulation in a human left coronary artery in its healthy and atherosclerotic states. Am. J. Physiol. Heart. Circ. Physiol. 296(6), H1969-1982.

Sharma, K, Bhat S.V., 1992. Non-Newtonian rheology of leukemic blood and plasma: are n and k parameters of power Law model diagnostic? Physiol Chem Phys Med NMR, 24, 307-312.

Soulis, J.V., Giannoglou, G.D., Papaioannou, V., Parcharidis, G.E., Louridas, G.E., 2008. Low-Density Lipoprotein concentration in the normal Left Coronary Artery tree. Biomed Eng Online, 17, 7-26.

Stangeby, D.K., Ethier, C.R., 2002. Computational analysis of coupled blood-wall arterial LDL transport. J. Biomech. Eng., 124(1), 1-8.

Wada, S., Karino, T., 2002. Theoretical prediction of low-density lipoprotein concentration at the luminal surface of an artery with a multiple bend. Ann Biomed Eng, 30, 778-791.

Zhao, W., Wang, X., Jiang, Y., Zhang, J., 2010. Non-Newtonian behavior of blood and arterial curvature influence variation of wall shear stress in stented artery. Vth European Conference on CFD,ECCOMAS CFD 2010, Lisbon, Portugal 14-17, June.